

ABSOLUTE VACUUM ULTRAVIOLET PHOTOABSORPTION CROSS SECTION STUDIES
OF ATOMIC AND MOLECULAR SPECIES: TECHNIQUES AND OBSERVATIONAL DATA

D.L. JUDGE and C.Y.R. WU
Space Sciences Center and Department of Physics
University of Southern California
Los Angeles, California 90089-1341

ABSTRACT

Absorption of a high energy photon ($> 6\text{eV}$) by an isolated molecule results in the formation of highly excited quasi-discrete or continuum states which evolve through a wide range of direct and indirect photochemical processes. These are: photoionization and autoionization, photodissociation and predissociation, and fluorescence. The ultimate goal of the study of these processes is to understand the dynamics of the excitation and decay processes and to quantitatively measure the absolute partial cross sections for all processes which occur in photoabsorption. In this paper, typical experimental techniques and the status of observational results of particular interest to solar system observations will be presented.

INTRODUCTION

The spectral region from 2 - 2000Å is called the vacuum ultraviolet radiation (VUV) because, even on a laboratory scale, electromagnetic radiation in this region is absorbed by air, and vacuum techniques are required. As is well known by planetary atmosphere scientists, this is also the wavelength range which is absorbed by all planetary atmospheres and, hence, is of major importance in determining atmospheric heating, photochemistry, and atmospheric structure.

To understand atmospheric structure and dynamics it is thus essential to accurately know the absolute total cross sections for all atoms and molecules which may play a significant role in determining the physical state of an atmosphere. It is also necessary to know the absolute and specific partial cross sections for the fragmentation products as well as their kinetic energy. Tabulations of much of the available data on such processes may be found in publications by Gallagher et al.,¹ Koch and Sonntag,² Hudson and Kiefer,³ Hudson,⁴ and Watanabe.⁵ Unfortunately, much of the early work on specific cross sections suffered due to a number of experimental difficulties. Early work on photodissociative ionization, for example, was carried out using magnetic sector

mass spectrometers which severely discriminated against short lived and/or energetic species. Thus, even the relative amounts of ions formed were not well established. Furthermore, such a technique provides no information about the state of excitation, except as can be inferred from energy conservation considerations.

During the past twenty years, however, much has been accomplished with respect to determining both total and partial absolute cross sections throughout the VUV. Such progress has been possible in large measure because of newly developed experimental techniques and technological advances. While an exhaustive in-depth review of the experimental techniques generally employed will not be given here, representative techniques used to obtain the data required for understanding atmospheric processes will be presented in later sections.

A schematic summary of the absorption and decay processes which can occur in the VUV is presented in Fig.1. As can be seen from the figure, ionization,

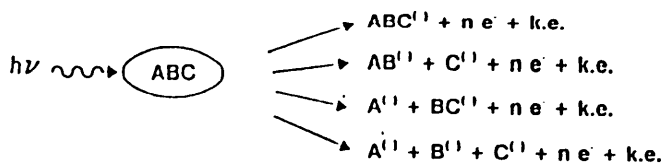


Fig.1. Molecular absorption and decay processes.

HERE, $i, j, k = (1, 2, \dots)$; and/or $0, \dots$

$$n = \begin{cases} 0 & \text{FOR NEUTRAL PROCESSES} \\ 1, 2, \dots & \text{FOR IONIZATION PROCESSES} \end{cases}$$

dissociation, excitation, or a combination of all three processes may occur. The products all appear in the atmospheric soup driven by the solar VUV radiation and can lead to complex atmospheric chemistry and dynamics. Fortunately, it is now technologically possible to determine the absolute cross sections for all of the reactions shown in Fig.1. In fact, absolute measurements of such processes are being obtained in various laboratories. Recent technological advances of particular importance to such comprehensive measurements are discussed in the next section.

INSTRUMENTATION ADVANCES

There have been several cleverly applied technical advances in the last two decades which have permitted a detailed understanding of many atomic and molecular processes. These advances fall into two categories: 1) Light source development and 2) Detector development. In both of these areas tremendous

progress has been realized.

Light Source Development

Pure continuum light sources for the VUV, particularly the extreme ultraviolet, were not available until the advent of dedicated synchrotron radiation sources. It is now possible for scientists around the world to have access to such sources and to thereby study absorption processes as a continuous function of photon energy. There are about twenty such facilities currently in operation, many of them providing continuum radiation down to wavelengths of a few Angstroms. Representative synchrotron source spectra are shown in Fig.2.

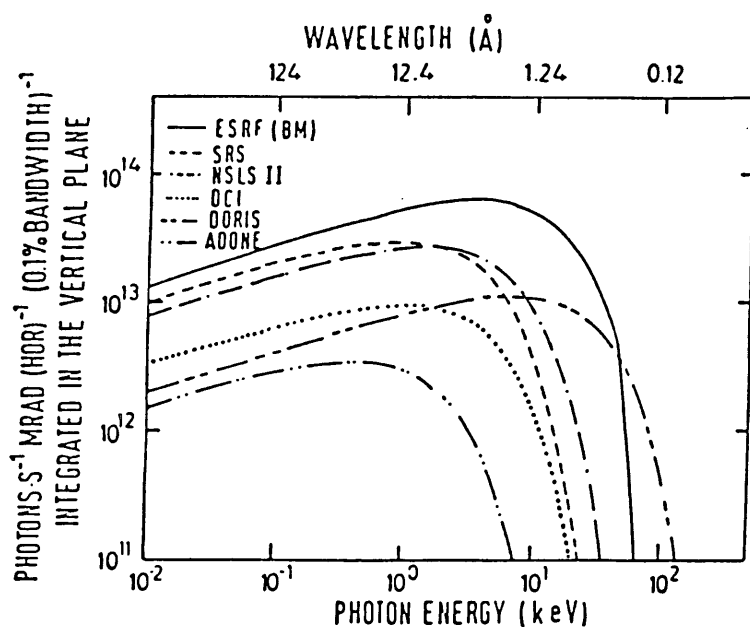


Fig.2. Intensity spectra for several storage rings used as synchrotron radiation sources.

Such sources provide a pure continuum of radiation, with intensities comparable to the average intensities available in conventional laboratory sources which, at best, cover limited wavelength regions and typically have both line and continuum features mixed. Using such mixed sources makes it difficult to measure true absorption cross sections except in regions of continuum absorption with no superposed structure. This is so because the bandwidth for which a monochromator is set generally corresponds not to the bandwidth of the incident source line but to the bandwidth for continuum radiation.

In addition to the synchrotron source another significant advance in light source capability has come from advances in laser technology. It is now possible to purchase lasers which are tunable over a significant wavelength region in the VUV. Nd:YAG tunable dye lasers with appropriate non-linear elements provide

useful radiation down to about 760\AA . The linewidth of such sources can be $<0.3\text{cm}^{-1}$ so that features as narrow as several m\AA can be resolved in the VUV. Such sources^{6,7} have been shown to have a VUV linewidth comparable to that previously available from a 6.5-m spectrograph. Thus, the prospect of carrying out high resolution spectroscopy in a conventional laboratory is now both possible and affordable in the window region of the VUV. This is also a particularly important region since it includes the spectral range where absorption by hydrocarbons, and other molecules present in the lower atmospheres of several planets, show significant diagnostic absorption features.

Detectors

To complement the improved light sources, photoelectric detectors have been highly developed and are now used almost exclusively in lieu of photographic recording. This has permitted a number of experimental advances which are now widely employed in both particle and electromagnetic detection. Fast photoelectric detectors (and short pulse light sources) permit direct measurement of lifetimes as short as ~ 1 ns. Synchronous detection of events has made it possible to identify correlated events, again on a time scale of several nanoseconds.

The development of photoelectric array detectors has been particularly important as a replacement for photographic plates in the focal plane of spectrometers. Such detectors have made it possible to greatly improve the speed with which a spectrum can be obtained. In addition, they also make it possible to follow the temporal and spatial evolution of dynamical processes in unimolecular systems, as well as in high density, collision dominated systems. Such detectors are commercially available as charge coupled detectors (CCD's), intensified CCD's (ICCD's), and resistive anode arrays.

The time scales for electric dipole and other transitions, in the absence of collisions, are given in Table I, and have been included as a reminder of the tremendous range of times of interest in the investigation of molecular processes. The temporal requirements imposed on laboratory instrumentation, both on the light sources and the detectors, are of course determined by such time scales.

An overview of the data obtained in photon-molecule interaction studies in the VUV is briefly described in the next section.

Table I Time Scale for Electric Dipole, Magnetic Dipole and Quadrupole Transitions for Photon-monomolecular Processes

Process	Type of Transition	Time (sec)
Excitation	Electronic - Electric Dipole	$\sim 10^{-16}$ - 10^{-18}
	Vibration - Electric Dipole	$\sim 10^{-13}$
	Rotation - Electric Dipole	$\sim 10^{-12}$
	Metastable - Magnetic Dipole	$\sim 10^{-12}$
	Metastable - Quadrupole	$\sim 10^{-9}$
Ionization	(Direct or Indirect)	$\sim 10^{-18}$ - 10^{-12}
Dissociation	(Direct or Indirect)	$> 10^{-13}$
Radiative Decay	Electronic - Electric Dipole	$> 10^{-9}$
	Vibrational - Electric Dipole	$> 10^{-4}$
	Rotational - Electric Dipole	$> 10^{-3}$
	Metastable - Magnetic Dipole	$> 10^{-3}$
	Metastable - Quadrupole	> 1

Absorption and Ionization Cross Section Measurements

The total absorption cross section at a given incident photon energy is a measure of the sum of the partial cross sections shown in Fig.1. At wavelengths shortward of the ionization limit of the gas of interest, electrons and ions are produced. The photoionization yield can be determined through measurement of the ions produced and/or photoelectron spectroscopy. A recent review of such measurements, primarily in the XUV ($\lambda \leq 1000\text{\AA}$), and a compilation of the absolute cross sections for a number of gases of planetary interest for molecular photoabsorption, and partial photoionization, is given by Gallagher et al.¹

The measurements discussed above have been concerned with the primary photoabsorption process and the initially formed products. The "final" products which evolve through predissociation, preionization, etc. are also of great interest. It is the final products, in fact, which in general are of the most importance in atmospheric chemistry. Most redistribution of energy within a molecular system occurs on a time scale which is short compared with the mean time between collisions, except for metastable states (see Table I).

To probe these final states, fluorescence spectroscopy provides a powerful tool. To identify excited final state fragments one can simply disperse the fluorescence and thereby determine the species formed, their states of excitation, and (from the brightness) the cross sections for the production of specific states down to the rotational level. To detect species which have been formed either in the ground state, or in a metastable state, the observation of scattered radiation from tunable laser sources provides an effective technique. The fluorescence technique has been pioneered by our group at USC and has proven quite useful for the determination of absolute cross sections for the production of final state products. Examples of final state identification for molecular fragments of particular planetary interest will be given in the next section as specific results of interest in planetary and cometary physics.

Another final state determination of particular interest to planetary atmosphere physics is the kinetic energy carried by the fragments produced. Such experiments have also been recently initiated in our laboratory. It has been found that quite a large kinetic energy is produced in both N and H fragments through photodissociation of N_2 and H_2 . Implications for the optical thickness of a planetary atmosphere as well as non-thermal escape may be seen in the observational data. Results of this recent work will be reviewed in the following section.

SELECTED LABORATORY RESULTS AND DISCUSSION

In the present section we show selected results of interest in planetary and cometary investigations. These are of four types: 1) Modest resolution absorption spectra showing the dependence of measured cross sections on temperature and spectral resolution, 2) Photofragment identification (through radiative decay observations), 3) Kinetic energy distribution of photofragments, 4) Photon sputtering of ice. These few observational areas have been selected for discussion because they are representative of the laboratory data base which is required to support solar system atmospheric studies. The chemistry, convection, radiative transfer, and general characteristics of planetary atmospheres are all coupled to the primary photoabsorption processes which are discussed.

Cross Section Data

With regard to the cross section data, item 1) in the above list, it is

a fact that the supporting laboratory spectroscopic data are almost always less complete and of lower quality than the flight observational data. This deficiency will become much worse as observational capability in other areas increases, for example with the launch of Space Telescope. As may be seen in Fig.3, data obtained at room temperature and low pressures are still incomplete,

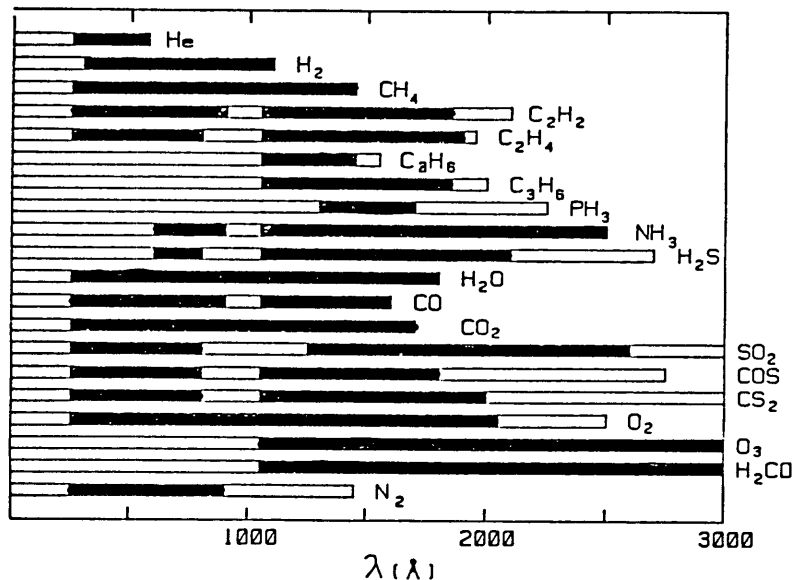


Fig.3. This figure summarizes the absorption region of the molecules of primary interest. The solid area indicates that gaseous photoabsorption cross sections have been measured as a continuous function of the incident photon wavelength.

and are virtually absent for other conditions of temperature, pressure, and relative abundance. Virtually all of the presently available absorption cross section data were taken at pressures, temperatures, and relative abundances very different from atmospheric conditions and are, therefore, of limited utility. It is known, for example, that when more than two kinds of molecules in a gas mixture absorb light in the same wavelength region, the total absorption cross section may become more complicated than merely the sum of the individual absorption cross sections, obtained at the usual laboratory conditions, i.e., 300°K and low pressure. The reasons are as follows: (i) at elevated temperature the population of higher vibrational levels (overtones and combination bands) may become significantly increased. This can result in a significant change in the amount of absorption at a given wavelength, and shift the effective ionization and dissociation thresholds. This in turn affects the penetration of solar ultraviolet radiation and ion production rates at high altitude,⁸ and the molecular lifetimes.⁹ The cross sections of molecules at low temperatures thus cannot be accurately obtained from the extrapolation of room temperature data, since at room temperature the absorption from vibrational and rotational levels other than the vibrationless ground state contribute to the observed cross

section. (ii) High pressure, up to several atmospheres, in an absorbing system can cause line broadening, line shifts, and pressure-induced transitions. The line shift may be to the blue or to the red of the spectral line, showing asymmetric broadening, while dipole-forbidden transitions become allowed transitions.^{10,11} (iii) Real atmospheres consist of a mixture of various molecules. As we know from (ii) the pressure effects may vary in nature depending on the characteristics of the collision constituents.¹² It is thus desirable to measure the cross sections of molecules under the conditions of the planetary atmosphere of interest. For example, to model the albedos of Jupiter, Saturn, and other planets, obtained from IUE data, Caldwell and Owen¹³ have pointed out the need for the absorption cross sections of PH_3 , H_2S , C_2H_2 , NH_3 and C_2H_6 in the 1600 - 2100Å spectral region, at temperatures varying from 300 to 150°K and absorber abundances varying from 0.2 - 5cm-atm. Unfortunately, very little progress has been made since this need was pointed out.

Continuing research using IUE data further indicates that cross sections for a number of complex hydrocarbons will soon be required. As an example, we review the IUE data of Jupiter¹⁴ in the 1400 - 1900Å region, shown in Fig.4. Since Jovian C_2H_2 dominates in the 1750 - 1900Å absorption region, a mixing ratio of 3×10^{-8} (Fig.4a) is required in order to obtain a good fit between observational data and model calculations.^{14,15} With this mixing ratio it is obvious that there must be additional absorbers present in the wavelength region shortward of 1750Å. If small amounts of allene (C_3H_4 , Fig.4b) and also cyclopropane (C_3H_6 , Fig.4c) are included in the model calculations¹⁴ an improved fit to the general variation of albedo with wavelength is obtained, although information on the positions and bandwidths of many features in the spectrum

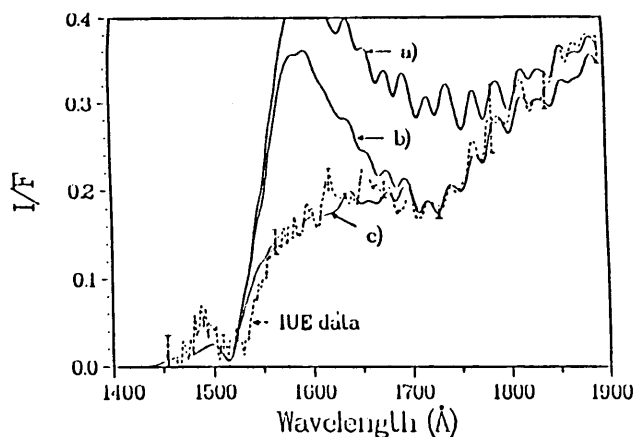


Fig.4. Dashed line: IUE data. (a) Model spectrum with C_2H_2 (mixing ratio 3×10^{-8} , C_2H_6 (2×10^{-6}) and CH_4 (1.7×10^{-3}) in Jovian stratosphere (0 to 100mbar) and the model of Goldstone and Yung (1983) for 100 to 60mbar. (b) Model spectrum as in (a) but including allene (7×10^{-10}). (c) Model spectrum as in (b) but including cyclopropane (8×10^{-9})

clearly needs to be improved. The fit is not good enough to prove conclusively that the identification of trace gases other than C_2H_2 is unique.

One strong possibility for the discrepancy in fine detail may be the fact that the molecular cross section data used in the calculations were measured at room temperature ($\approx 300^\circ K$), which is very different from that in the Jovian atmosphere ($\sim 150^\circ K$) at the absorbing level. The temperature effect may well explain why the IUE data show a spectral bandwidth narrower than model calculations predict. Further, inclusion of the temperature effect on the molecular cross sections will accordingly change the required mixing ratios of various absorbers. It is therefore clear that such measurements are required and will contribute to our current understanding of planetary atmospheres.

Absorption Cross Section for Acetylene

In the absorption cross section discussion presented below we will only discuss the temperature dependence of the absorption cross section of C_2H_2 (Acetylene) in a wavelength region of significant absorption in the outer planets. Figures 5 and 6, respectively, show our recently obtained absolute cross sections of C_2H_2 in the 1530 - 1930Å region measured at room temperature ($295^\circ K$) and at $115^\circ K$.

As can be seen from Fig.5, the complex absorption features are clearly superimposed on a broad "continuum" (or "continua"), with the most intense features being the 3_0^6 and 3_0^7 peaks. Under room temperature conditions, the largest cross section value of the B - X transition is 1.7Mb ($1Mb = 10^{-18}cm^2$) for

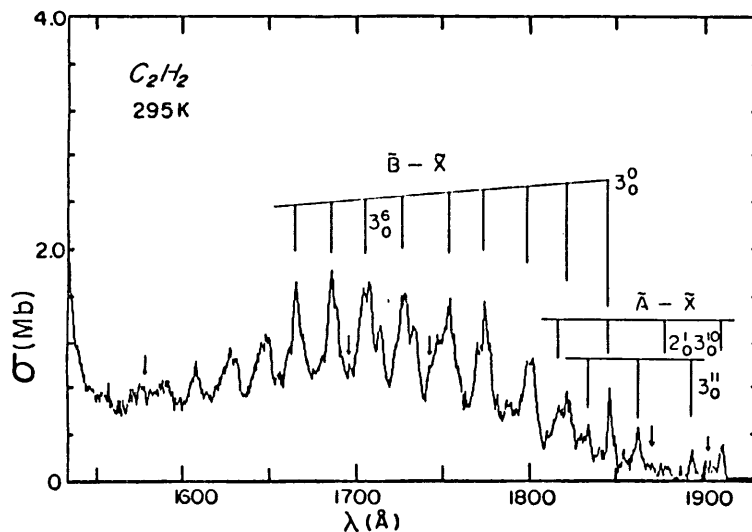


Fig.5. The absolute photoabsorption cross section of C_2H_2 in the 1520 - 1900Å region. The data are obtained with a spectral bandwidth (FWHM) of 0.8\AA and at a temperature of $295^\circ K$.

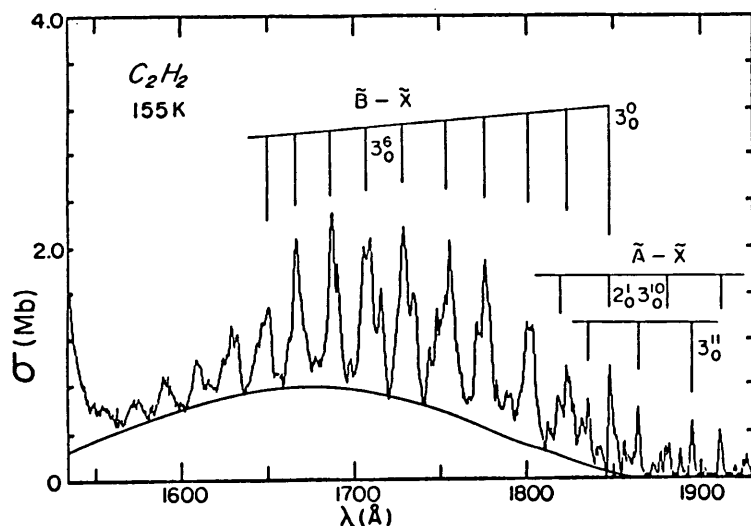


Fig.6. Same as Fig.5 except the cross section data are obtained at a temperature of 155°K.

the 3_0^6 peak. The smallest is less than 10^{-19}cm^2 for the $\bar{A} - \bar{X}$ transition on the long wavelength side.

Clearly the low temperature cross sections obtained at 155°K are quite different from those measured at room temperature. As one can see from Fig.6, the peak cross sections of the 3_0^5 , 3_0^6 and 3_0^7 bands are about equal in magnitude (i.e., 2.2 Mb) with 3_0^7 being the largest peak. The drop in peak cross sections from the 3_0^7 peak to the 3_0^n with $n \geq 8$ becomes quite pronounced. Such a sudden drop can be due to vibrational predissociation through perturbations.

The resolution of the low temperature spectrum is "apparently" (but only apparently) better than that obtained under room temperature conditions. Many broad features become resolved into several peaks. The most striking effect on the absorption profiles occurs in the 1580Å region and in the wavelength region longward of 1800Å. Several unmeasurable band heads of the $\bar{A} - \bar{X}$ transition under room temperature conditions clearly become identifiable peaks at low temperature. These peaks are the $2_0^1 3_0^n$ progression with $n=8$ and 7 and the 3_0^n progression with $n=8$ and 9. Further, the sharpness of the peaks allows a better wavelength measurement and, hence, a better determination of the vibrational constants which are applicable to high quantum numbers. Those peaks marked by an arrow as shown in Fig.7 appear to be hot bands. Considering a polyatomic molecule as large as C_2H_2 , it is surprising that hot band absorption is apparently quite sparse in this spectral region, particularly in the region of the $\bar{B} - \bar{X}$ transition.

To summarize the temperature dependent studies, it is found that the low temperature cross section values at absorption peaks increase by 10% - 40% while

those at absorption valleys decrease by as much as 30%, when compared to the room temperature measurement. The cross section values of the "continuum" absorption are also correspondingly reduced somewhat. The application of the new low temperature data to the interpretation of Saturn's albedo has been discussed in the Conference Proceedings by Caldwell et al.

An example of how the low resolution also affects such cross section data may be found in the review by Hudson.⁴ Figure 7 shows $n\sigma l$ vs. $\ln(A_0/A)$ for various ratios of α ($\alpha = \Delta\lambda/\Delta L$). Here n is the gas density in an absorption cell of length l , the cross section is σ , A_0 and A are the incident and transmitted intensities, respectively, $\Delta\lambda$ is the monochromator bandwidth for a continuum background, and ΔL is the Lorentz full width at half maximum (FWHM) for an absorption feature. If the resolution of the instrument is significantly less than the true width of the structure (spectral features) being observed then the true cross sections, σ_T , will be measured. If $\sigma_T = \bar{\sigma}_T$, the average cross section, a straight line of slope one would be obtained in the above plot. If $\alpha \leq 0.3$

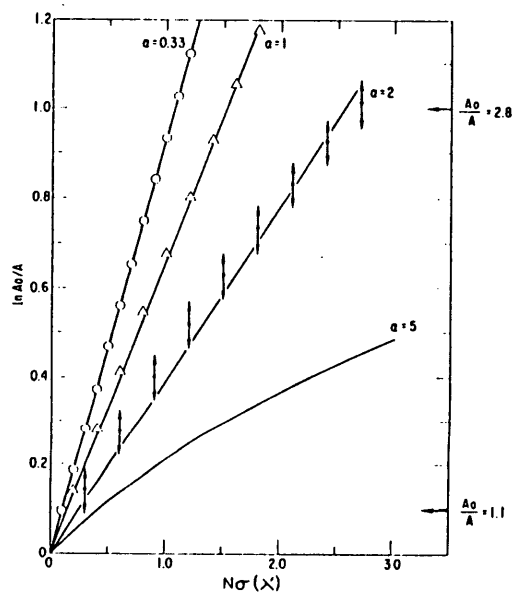


Fig.7. Calculated values of $\ln(A_0/A)$ vs. $N\sigma(\lambda')$ for four values of α ($\alpha = \Delta\lambda/\Delta L$) assuming a Lorentz line shape.

measurements of σ_T to an accuracy of $\leq 1\%$ are obtained. For $\alpha=1$, the measured cross sections, i.e. $\bar{\sigma}_T$, will be only $\sim 70\%$ of σ_T . As might be expected, particularly in the early literature, it is often not clear what the effective resolution of the instrument and light source combination actually was. All cross sections should thus be carefully considered before they are used in modelling calculations. Remeasurement of many of the cross sections in the literature will unfortunately need to be carried out. In any case, most of them should be remeasured for planetary atmosphere applications since room temperature

data are only applicable to a very limited range of planetary atmosphere conditions.

Photofragment Identification

Photofragments, as discussed earlier, can be identified by a variety of techniques. Photoelectron spectroscopy provides data on the initial fragments formed in ionization processes. As internal rearrangements occur, the final products may be different from the initial state products. In addition, neutral fragments are not detected by such techniques.

A dispersed fluorescence spectroscopy technique which detects and identifies the final state products was developed at USC in the early 1960s. In such work both the photons incident on the gas of interest and the emitted photons are dispersed. In this way excited fragments ultimately produced in photoabsorption processes are observed and the absolute partial cross sections for their production are determined. As an example of the results which can be obtained from such work, let us consider the photoabsorption and photofragmentation spectrum of H₂O (see Fig.8).

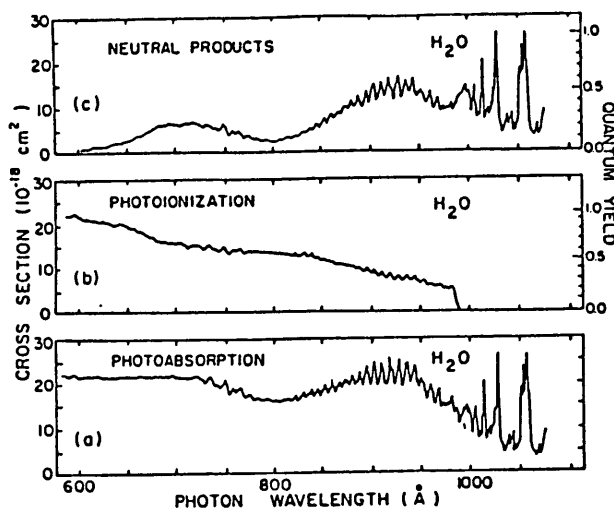


Fig.8. The absolute cross sections of (a) photoabsorption, (b) photoionization, and (c) neutral products in the 600Å (20.66 eV) - 1200Å (10.33 eV) region.

H₂O Fragmentation

The photoabsorption and photoionization cross sections of H₂O in the 600 - 1100Å region are shown in Figs.8a and 8b, respectively. In this region significant dissociation into neutral fragments is clearly evident since the total absorption and ionization cross sections are not equal to each other. For wavelengths shorter than ~600Å, the photoionization cross section is equal to the total photoabsorption cross section; i.e., the photoionization efficiency

of H_2O is unity. By subtracting the ionization cross section from the total absorption cross section, we obtain the cross section for neutral products which is shown in Fig.8c. The neutral products include ground, metastable, and excited state neutral photofragments. The quantum yield, which is defined as the ratio of the partial cross section of interest to the total photoabsorption cross section, for the respective neutral products and ionization is indicated on the right-hand side of Figs.8b and 8c. As can be seen, the maximum quantum yield for producing the neutral products is 1.0, ~ 0.6 , and ~ 0.3 for the wavelength range > 984 , $800 - 984$, and $600 - 800\text{\AA}$, respectively.

It is well known that fluorescence from the excited states of the neutral H_2O molecule and parent H_2O^+ ion have rarely been observed.¹⁶ The fluorescence quantum yield of the first excited state of the $\text{H}_2\text{O}^+(\text{A } ^2\text{A}_1)$ ion is extremely small. The second excited ion state $\text{B } ^2\text{B}_2$ is not known to fluoresce, while the third excited ion state $\text{C } ^2\text{A}_1$ is completely predissociated.¹⁶ In contrast with this, the fluorescence from excited photofragments, especially the H Balmer series and $\text{OH}(\text{A} \rightarrow \text{X})$, is intense and has high quantum yields. Since the OH fragment is of particular interest a brief description of the OH observations follows.

The partial cross section for producing the $\text{OH}(\text{A} \rightarrow \text{X})$ emission has been measured at several discrete primary photon wavelengths longer than 760\AA using an atomic line emission source. The band contours of the (0,0) band are shown in Fig.9. A fraction of the photon excitation energy is converted into internal energy. It is quite evident from Fig.9 that higher rotational energy levels are excited as the incident photon energy is increased.

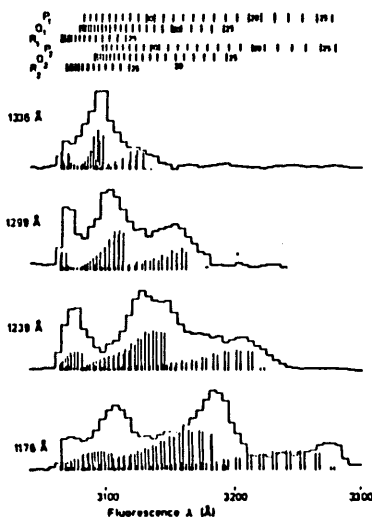


Fig.9. The $\text{OH}(\text{A } ^2\Sigma^+ \rightarrow \text{X}^2)$ fluorescence spectra in the $\lambda\lambda$ 3060 - 3300 \AA region produced at various primary photon wavelengths, compared with the theoretical synthetic rotational spectra of the $\text{OH}(\text{A } ^2\Sigma^+, \nu'=0, J' \rightarrow \text{X}^2, \nu''=0, J'')$ band, for which the radiation rates are indicated as vertical lines. The positions of the rotational lines for the six intense branches of the OH band are also indicated at the top of the figure.

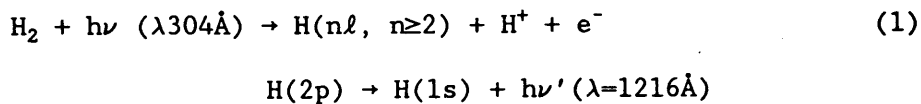
The OH(A→X) fluorescence excitation functions in the 180 - 760Å and 1050 - 1350Å regions have also been obtained using a synchrotron radiation source. In the former spectral region, the maximum partial cross section occurs at about 703Å and is $3.4 \times 10^{-20} \text{cm}^2$, giving a quantum yield of 2×10^{-3} . Shortward of 700Å the partial cross section decreases sharply to a magnitude of $\sim 5 \times 10^{-21} \text{cm}^2$.

Atomic hydrogen fragments associated with the dissociation of H₂O have also been observed as well as upper limits to the production of atomic oxygen and molecular hydrogen, but a discussion of these results is beyond the purpose of the present work.

Kinetic energy measurements of molecular fragments

The kinetic energy distribution of atomic fragments is particularly important since these fragments may have considerable kinetic energy, thus modifying atmospheric reaction rates and escape rates. In the example given below, the processes which correlate with the photo-production of an excited neutral hydrogen atom and a hydrogen ion are discussed.

Specifically, we have utilized a fluorescence photon-photoion coincidence technique to study the processes:



We have carried out the experiment by measuring the coincidence time delay between the detection of the emission of a H Ly α photon and a H⁺ ion produced through photon excitation of H₂ at a photon wavelength of 304Å. It should be noted that from energy and momentum conservation the excess excitation energy, defined as the difference between the incident photon energy and the threshold energy for the process of interest, minus the kinetic energy of the photoelectron will be equally divided between the excited H(n ℓ) atom and the H⁺ ion. Thus, the kinetic energy distribution measured for the H⁺ ions is equivalent to that for the excited H(n ℓ) atoms.

The experimental data are obtained by means of a coincidence detection system.¹⁷ A true coincidence count results when the output of the TAC is turned-on by a photon pulse, e.g., $\lambda = 1216\text{\AA}$, and turned-off by the H⁺ pulse. Both the 1216Å photon and the H⁺ ion have to be produced from the same H₂ molecule. Only under these conditions would the process indicated in Eq.(1) show up preferentially in a specific range of time delay, Δt , resulting in the observed

peak. False coincidences result from everything else and would show up as background since they are random events.

From Fig.10 we see a clear increase in the coincidence counts at a time delay of $5.6 \mu\text{s}$. After reaching a maximum at $\Delta t = 6.5 \mu\text{s}$ the coincidence counts start to slowly decrease, followed by a much weaker peak in the $7.7 - 8.5 \mu\text{s}$ region. The asymmetry obvious in the shape of the major peak suggests that it may arise from more than one dissociative excitation process. The kinetic energy distribution obtained is shown in Fig.11. As one can see, the H^+ ions (and excited H atoms) produced through photoexcitation of H_2 at 40.8 eV possess kinetic energies ranging from 1.2 to 7.5 eV .

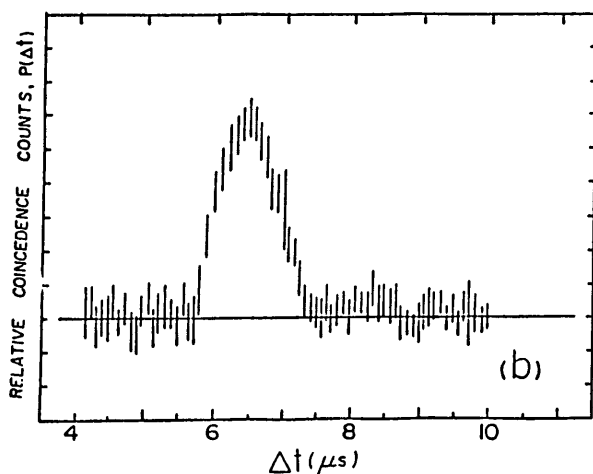


Fig.10. Relative coincidence counts vs. time delay.

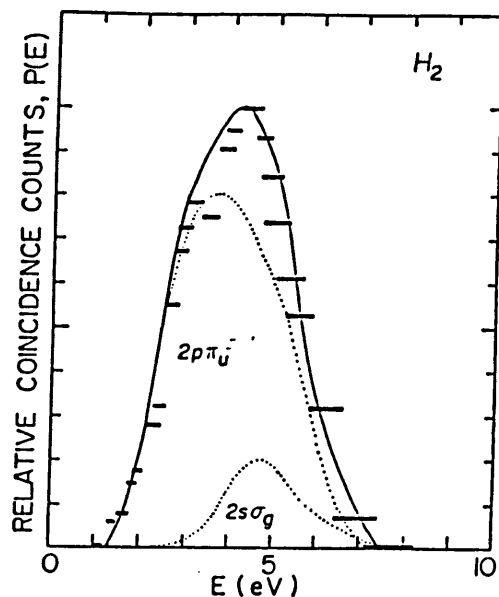


Fig.11. Relative coincidence counts vs. energy.

Using He II 304\AA (40.8 eV) photons, Gardner and Samson¹⁸ found that the direct dissociative ionization of H_2 involving the $2p\sigma_u$ state accounts for 44.4% of the total signal while dissociative ionization involving states of higher energy than the $2p\sigma_u$ accounts for the remaining 55.6% . Combined with the present results, we now find the relative partial cross section for dissociative photoionization of H_2 to be the following:

$$2p\sigma_u : 2p\pi_u : 2s\sigma_g = 1.0:1.0:0.25 \quad (2)$$

The partial cross section for producing H Ly α emission through photoexcitation of H_2 has recently been reported by Glass-Maujean.¹⁹ As

indicated in Eq.(1), the present experiment measures cross sections related to those of Glass-Maujean. After subtracting the contribution from the two-electron excited states, $Q_1 \ ^1\Pi_u(1)$ and $Q_2 \ ^1\Pi_u(1)$, the partial cross section for producing H Ly α from H₂ at 40.8 eV is $4.5 \times 10^{-20} \text{cm}^2$ (see, Fig.3 of Ref.19). If we assume, as Glass-Maujean implicitly did, that the partial cross section in the energy region higher than 40 eV is solely due to the $^2\Pi_u$ state, i.e., the $2p\pi_u$, then we can deduce the partial cross section for the dissociative photoionization of the $2p\sigma_u$, $2p\pi_u$, and $2s\sigma_g$ states to be 3.6×10^{-20} , 3.6×10^{-20} , and $9.0 \times 10^{-21} \text{cm}^2$, respectively.

From the above results it is thus clear we have demonstrated that the present technique is a powerful tool for studying dissociative photoionization excitation processes. It allows us to study states correlating only with excited neutral and ion photofragments. The kinetic energy distributions obtained from the present work show that the H⁺ ions as well as the H atoms produced possess high kinetic energies. For an H atom, the escape velocity on Earth is 11.179 km/s which is equivalent to a kinetic energy of 0.65 eV. Since solar extreme ultraviolet photons at 304Å, and shortward, are absorbed in the Earth's upper atmosphere, it is clear that the presently observed photodissociative ionization of H₂ contributes to the non-thermal escape of atomic hydrogen from the Earth's atmosphere.

Photon sputtering of ices

Investigations of the efficiency of photon sputtering of ices have been extremely limited, and the available data are quite incomplete and inconclusive (Haff et al.²⁰). The only measurements of adsorbed gases which exist are those by L. Greenberg²¹ using a broadband UV (~ 2000 - 2750Å) photon source. The molecular ices which he studied have virtually no absorption in the case of H₂O, CH₄, and CO₂, and little absorption in the case of CS₂, O₂ and NH₃. Not surprisingly, he found a desorption quantum yield of $\sim 10^{-6}$, see Table II.

Given the complete lack of data in the strongly absorbing region of these molecular gases it is clear that such data are sorely needed. We have accordingly initiated experiments to measure the required sputtering rates. The first data have just been obtained on water ice at 584Å and the preliminary results are included in the Conference Proceeding in a paper by Wu and Judge. This report, it should be noted, only addressed the charged particles which were ejected. It should also be noted that the yield of positive ions above, at

Table II Photodesorption Yield for Physically Adsorbed on Quartz

Yield	Molecule	Temp(K)	k(P)	Comment	Ref.
$\sim 1 \times 10^{-5}$ ^{a)}	CS ₂	77	Broadband 2000-2750Å from a Hg-Xe lamp	abs. <2200P $\sigma \geq 8 \times 10^{-22} \text{cm}^2$ ^{b)}	Greenberg [1973]
$\sim 1 \times 10^{-6}$ ^{a)}	CO ₂	"	"	no abs.	"
"	O ₂	"	"	Herzbergband $\sigma \geq 10^{-23} \text{cm}^2$	"
"	CO	"	"	no abs.	"
$10^{-7} \sim 10^{-8}$ ^{a)}	H ₂ O	"	"	"	"
"	NH ₃	"	"	abs <2150Å $\sigma \geq 1.5 \times 10^{-17} \text{cm}^2$ ^{c)}	"
"	CH ₄	"	"	no abs.	"
1.3×10^{-2}	I ₂	"	5900Å dye laser	Spin-forbidden Transition (B-X); $\sigma = 1.2 \times 10^{-16} \text{cm}^2$ ^{c)}	Bourdon et al. [1982]
4.8×10^{-4}	"	"	4880Å Ar ⁺ laser	" ; $4.0 \times 10^{-16} \text{cm}^2$ ^{c)}	"
1.8×10^{-1}	Br ₂	60	5500Å dye laser	" ; $3.8 \times 10^{-20} \text{cm}^2$ ^{c)}	"
$< 9.2 \times 10^{-5}$	"	20	"	"	"
2.9×10^{-2}	Cl ₂	60	4880Å Ar ⁺ laser	" ; $3.8 \times 10^{-21} \text{cm}^2$ ^{c)}	"
$< 1.5 \times 10^{-5}$	"	20	"	"	"

a) According to Bourdon et al. [1982], those yields measured by Greenberg should be $\sim 10^{-10}$. b) Gas phase data taken from Wu and Judge [1981b]. c) Solution data taken from Mellor [1963].

584Å, was a factor of 100 higher than the total yield reported by Greenberg.²¹

In order to appreciate the spectral range where photon sputtering should be important, it should be noted that the molecular ices listed above are like electrical insulators with electronic band gaps of ≥ 10 eV. Because of the lack of conduction electrons both the electrical conductivity and the thermal conductivity in these ices are poor. This lack of free electrons in the ices enhances the probability that energy deposited in electronic excitations will be converted partly to translational energy of the excited icy molecules and thereby contribute to the sputtering efficiency.

The desorption rate strongly correlates with the excitation of electronic

states of the adsorbed molecule which is physisorbed and/or chemisorbed on the substrate. Thus, it is clear that the low desorption yields measured in Greenberg's experiment²¹ are not surprising, as neither the electronic states of the adsorbed molecular ices, nor the substrate, significantly absorb the incident long wavelength UV photons. Further, it is highly probable that the $\sim 10^{-1}$ yields in the halogen photon desorption experiments reported by Bourdon et al.²² may show a significant increase if electric-dipole allowed transitions were to be excited rather than the spin-forbidden processes which they observed. As can be seen from Table II, a wide range of desorption yields are possible, depending on the molecule and the photon energy.

In the work just begun at USC, strong transitions involving Rydberg states of H₂O ices will be excited using VUV/EUV photons. The substrates which will be used are LiF and sapphire, and are transparent for $\lambda > 1050\text{\AA}$, and $> 1410\text{\AA}$, respectively. Additional contributions to the desorption rate may be observable if the substrate absorbs the incident photons.

Since the sputtered products include both neutral particles and ions a variety of experimental techniques are required for their detection. Namely, (a) excited particles will be detected by a fluorescence photon counting technique, (b) ions will be detected by a mass spectrometer, (c) neutral particles will be detected by a selective photoionization mass spectrometer, and (d) certain special radicals and ground state species will be detected by a laser-induced fluorescence technique.

CONCLUDING COMMENTS

It is clear that experimentalists working in support of the planetary atmospheres program must endeavor to fill the data voids in the research areas discussed in this report. There is almost no absorption cross section data available which is truly representative of the temperature, pressure, and mix of gases actually encountered in planetary and cometary environments. For those processes which occur in the lower strata of planetary atmospheres, it is crucial that cross section data at temperatures at least as low as 50°K be obtained. It is, of course, only the long ($\lambda \geq 1000\text{\AA}$) and short ($\lambda \leq 100\text{\AA}$) wavelength VUV radiation which reaches the lower altitudes where such temperatures typically occur.

The upper atmospheres of planets are normally hot (Mars being a rather notable exception, as well as Venus on the night side) with thermospheric

temperatures of $\sim 1000^\circ\text{K}$. The absorption spectrum of gases at such high temperatures is, of course, quite different from room temperature and/or low temperature spectra. A rather dramatic example of this may be seen in the molecular oxygen absorption spectrum of Hudson and Carter²³ as shown in Fig.12 where the temperature values are 300, 600, and 900°K .

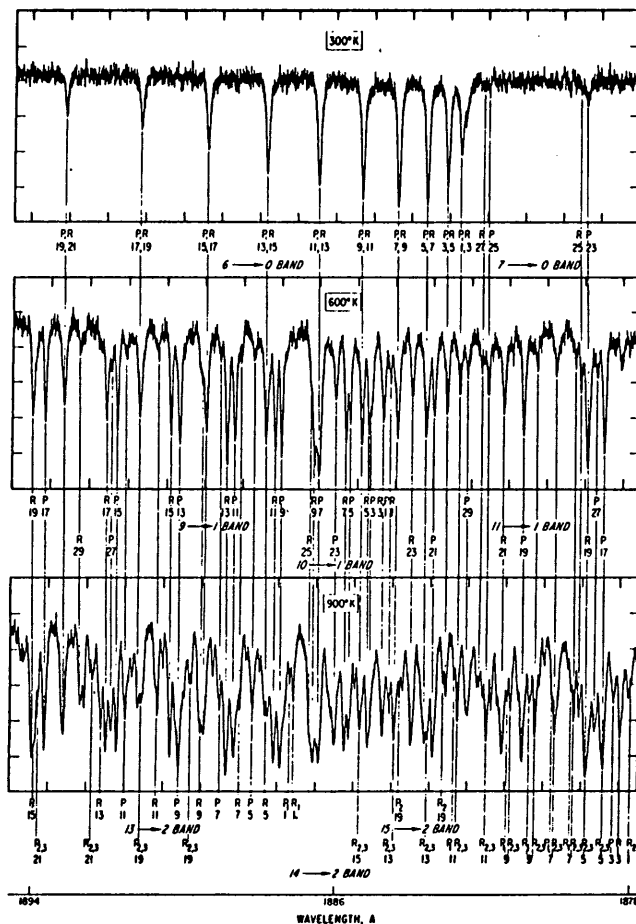


Fig.12. Absorption by molecular oxygen between 1878 and 1894Å at 300, 600, and 900°K .

All of these data, i.e., low and high temperature data, with and without buffer gases, must be obtained at high resolution in the structured regions. Spectral resolution of the order of $\sim \text{m}\text{\AA}$ is required to approach the linewidth of the absorbing atoms and molecules in planetary atmospheres in the regions of significant structure in the absorption spectra.

Product identification of the species formed in photoabsorption is another data set which is required in order to correctly interpret atmospheric processes. Since the chemistry which occurs in planetary atmospheres is crucially dependent on the state of excitation of the reacting species, the absolute cross sections for the formation of all product species must be determined. In such work, significant progress has been realized. However, the identification of, and

absolute cross sections for, the production of important metastable and ground state species remains in a very early state of development. Here, laser induced fluorescence techniques can be quite useful in resonance scattering identification or, in the case of metastable species, by exciting them to higher states from which they can fluoresce, and thereby be detected.

The measurement of photofragment kinetic energies is also an area where much remains to be done. Since non-thermal escape may be an important loss process for exospheric gases, it is essential that the kinetic energies for exospheric species be accurately measured as a function of wavelength, at least for the major solar emission lines in the VUV. The optical thickness of an atmosphere also depends on the kinetic energy of the atmospheric species and so radiation transfer calculations require data on the production rate of hot atoms.

Another area which was not discussed in this review is the lack of absolute absorption and fragmentation cross section data for radicals. This area is particularly devoid of data because the experimental techniques required are particularly demanding. Such research, however, is also quite important and should be vigorously pursued since radicals are highly reactive species.

Finally, photon sputtering of ices has been briefly discussed here because it may produce gases which are important constituents of planetary environments. As indicated earlier, this type of research has been almost completely ignored and must be investigated down into the soft X-ray region of the solar output. Non-thermal escape (sputtering) processes may well be far more significant than thermal processes alone.

While the above review was by no means exhaustive it has discussed the major deficiencies in the experimental data base relevant to the primary interactions of VUV photons with planetary gases (and solids).

Acknowledgments - This work was supported by NASA Grant #NGR-05-018-180. We are also grateful to the staff of the Synchrotron Radiation Center of the University of Wisconsin where much of the work presented here was obtained. The Synchrotron Radiation Center is supported by the National Science Foundation.

References

1. Gallagher, J.W., C.E. Brion, J.A.R. Samson, and P.W. Langhoff, "Absolute Cross Sections for Molecular Photoabsorption Partial Photoionization, and Ionic Photofragmentation Processes", *J. of Phys. and Chem. Ref. Data*, 17, 9 (1988).
2. Koch, E.E., and B.F. Sonntag, "Synchrotron Radiation", Topics in Current

Physics, 10, ed. C. Kunc, (Springer-Verlag, Berlin: 1979).

3. Hudson, R.D., and L.J. Kieffer, "The Nature of Stratosphere of 1974", CIAP Monograph 1. Department of Transportation Climatic Impact Assessment Program, Chap. 5 - 156, (1975).

4. Hudson, R.D., "Critical Review of Ultraviolet Photoabsorption Cross Sections for Molecules of Astrophysical and Aeronomic Interest", Nat. Stand. Ref. Data. Ser., NBS-38 (U.S. Government Printing Office, Washington, D.C.: 1971).

5. Watanabe, K., Adv. Geophys., 5, 153 (1958).

6. La Roque, P.E., R.H. Lipson, P.R. Hermann, and B.P. Stoicheff, J. Chem. Phys., 84, 6627 (1986).

7. Marinero, E.E., L.T. Rettner, R.N. Zare, and A.H. Kung, Chem. Phys. Lett., 95, 486 (1983).

8. Hunten, D.M., and M.B. McElroy, J. Geophys. Research, 73, 2421 (1968).

9. Stief, L.J. Molecules in the Galactic Environment, eds. M.A. Gordon and L.E. Snyder, 313, (John Wiley and Sons, N.Y.: 1973).

10. Welsh, H.L., M.F. Crawford, and J.L. Locke, Phys. Rev., 76, 580 (1969).

11. Lutz, B.L., J. Chem. Phys. 51, 706 (1969).

12. Wu, C.Y.R., and W.C. Stwalley, Phys. Rev., A18, 1066 (1978).

13. Caldwell, J., and T. Owen, Newsletter of Laboratory Spectroscopy for Planetary Sciences, 11, NASA Ames Research Center, (1981).

14. Wagner, R., J. Caldwell, T. Owen, S.J. Kim, T. Encrenza, and M. Combes, ICARUS, 66, 222 (1985).

15. Gladstone, G.R., and Y.L. Yung, Astrophys. J. 266, 415 (1983).

16. Wu, C.Y.R., and D.L. Judge, J. Chem. Phys. 89, 6275 (1988).

17. Wu, C.Y.R., T.S. Chien, and D.L. Judge, J. Chem. Phys. (in press, 1989).

18. Gardner, J.L., and J.A.R. Samson, Phys. Rev. A12, 1404 (1975).

19. Glass-Maujean, M., J. Chem. Phys. 85, 4830 (1986).

20. Haff, P.K., A. Eviatar, and G.L. Siscos, ICARUS, 56, 426 (1983).

21. Greenberg, L.T., in IAU Symposium 52, Interstellar Dust and Related Topics, eds. J.M. Greenberg and H.C. Van der Hulst (Dordrecht: Reidel; 1973).

22. Bourdson, E.B., R.H. Prince, and W.W. Dulay, Astrophys. J. 260, 909 (1982).

23. Hudson, R.D., and V.L. Carter, J. Opt. Soc. Amer., 58, 1621 (1968).